Algerian Journal of Research and Technology
https://doi.org/10.58681/ajrt.26100103
A.J.R.T Volume 10 (N°01) (2026) 19- 34

Integrated Structural, Petrophysical, and Petrographic Characterization of the Chinguetti Field, Mauritanian Coastal Basin

B. Dahmane[1], L. Aliouane[1]

[1]*Earth Physics Laboratory, Faculty of Hydrocarbon and Chemistry, M'Hamed Bougara University of Boumerdes, Boumerdes, Algeria.*

***Corresponding author:** dahmane.bah@univ-boumerdes.dz

Received. February 15, 2026. Accepted. June 13, 2026. Published. July 25, 2026

DOI: https://doi.org/10.58681/ajrt.26100103

Abstract. The Chinguetti Oil Field located offshore North West Africa, represents a structurally complex hydrocarbon system developed over a salt-cured diapir and strongly influenced by fault-driven compartmentalization. The field is a faulted domal anticline developed above an underlying salt diapir within the deepwater Mauritanian Basin. The structure is defined as a faulted domal anticline, dominated by a major east–west trending normal fault with significant throw, accompanied by radial faulting related to halo kinetic activity. These structural elements subdivide the field into distinct compartments, as evidenced by variations in fluid contacts and pressure behavior between wells. Fault seal analysis indicates that only faults with sufficient displacement contribute to effective compartmentalization, whereas smaller-scale and sub seismic faults may significantly influence fluid flow behavior. Hydrocarbon charge is linked to Cenomanian–Turonian source rocks, with migration facilitated by vertical pathways along salt domes. This study integrates 3D seismic sections with petrophysical well logs and petrography SWC data to constrain the geological framework, identify potential reservoir targets, and evaluate reservoir quality alongside the associated uncertainty and architectural complexity. The study integrates Posts TM seismic data, well-log interpretation, petrophysical analysis, and core-based petrography to characterize the structural and reservoir framework of the Chinguetti Field. Shale volume, porosity, hydrocarbon saturation, and net-to-gross were evaluated from well logs, while SWC and MSCT samples were analyzed using thin-section petrography, SEM, XRD, and grain-size analysis. The integrated workflow assesses reservoir compartmentalization, permeability uncertainty, and the influence of structural and depositional heterogeneity on reservoir quality and connectivity.

Keywords. MSGBC basin, Chinguetti field, Faults, gamma-ray, Porosity, Permeability, Petrography

INTRODUCTION

The NW African margin of the Central Atlantic has two major salt basins, the Moroccan and the Mauritanian which part of the MSGBC basin, and contain the Central Atlantic Magmatic Province (CAMP) (Tari et al., 2003; Davison, 2005; Vear, 2005, Dahmane et al., 2025; Péron-Pinvidic and Manatschal, 2009). Chinguetti-1 targeted Early Miocene, mid-slope, channelized turbidity reservoir sequences draped over a detached salt diapir. The well discovered the Chinguetti field and successfully proved a working petroleum system associated with the deepwater salt play in the Mauritanian basin (Fig. 1). The Chinguetti field structure is a faulted domal anticline developed over an underlying salt diapir. The faults are radial and concentric, dominated by a complex, roughly east-west, main fault that appears to be the oldest (Alsop et al., 2018). The faulting of the field has produced compartmentalization and perched fluid contacts across the structure and at least three different oil–water contacts (OWCs) are interpreted. The reservoir sediments comprise several point-sourced turbidity slope apron fan systems, each deposited as canyon fill, characterized by axial meander belts of high sinuosity channels/levees, developed within laterally adjacent marginal over bank deposits comprising thin sands, silts and mudstones. These episodes of turbidity canyon fill are more or less separated by laterally continuous hemi pelagic shale’s.

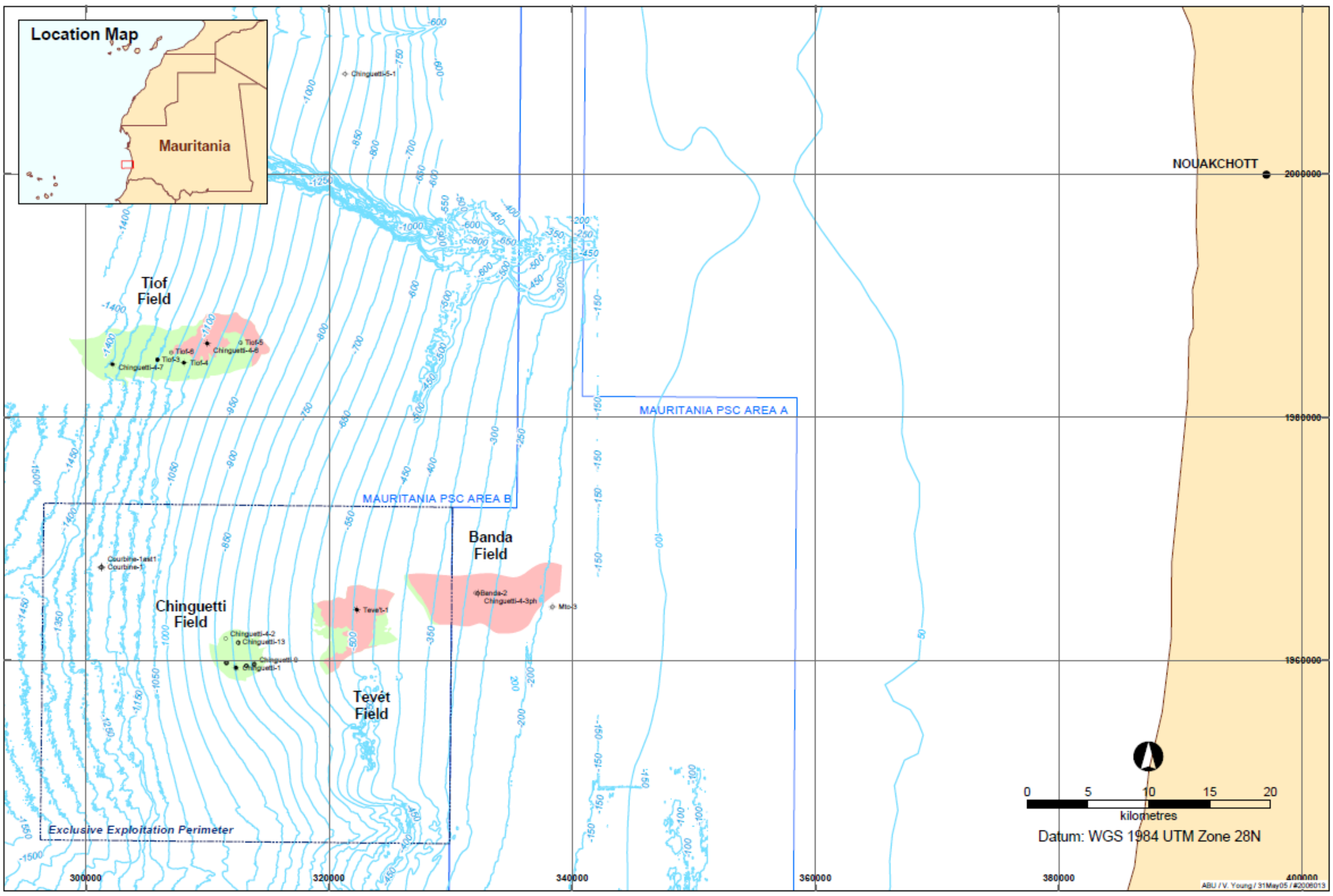

Fig.1. Chinguetti field Location map.

This study aims to constrain the lateral extent of salt structures across the Coastal basin and to elucidate the role of salt sheets and diapers in controlling fault development and fracture system architecture, to better understand the field geology, and reservoir Connectivity system. The Tarim Basin represents an analogous case to the studied reservoir (Bian et al., 2022). Comparatively few studies have examined salt fault compartmentalization (in the Saharan flexure of eastern Algeria and the Kazerun Fault Zone in the Zagros fold belt of southwestern Iran), despite analogous investigations in the Gulf of Mexico and other regions. Several studies have addressed Faults related salt tectonic systems (Letouzey et al., 1995; Letouzey and Sherkati, 2004). The field is divided into multiple compartments by faulting. At least three main compartments are defined by distinct fluid contacts. Additional smaller compartments are associated with minor and sub-seismic faults. Major faults are explicitly picked, while smaller faults are represented as transmissibility features. These features imply increased risk for additional compartmentalization with potentially a serious impact on both recovery and flow rates from these low NTG areas (As evidenced in Fig. 2) (Dahmane et al., 2025). The reservoirs were found to be more complex and compartmentalized than initial expectation, and hence production performance was poorer than initially forecasted. Production performance indicated that the reservoir extent was limited by the presence of more faults than earlier anticipated. More radialN-S faults indicated with E-W baffle faults in SE sector, suggested by E-W anisotropy.

Fault sealing behavior is a critical control on reservoir performance. Analysis indicates that faults with throws exceedingly approximately 10–20 m have the potential to act as effective seals, particularly where shale-rich intervals are juxtaposed across fault planes. Conversely, smaller faults are interpreted as largely transmissive. The primary objectives of the prospect were Middle Miocene to Pliocene amalgamated channel sands, which had not been encountered in previous wells. By their very nature sub-seismic faults are not imaged directly from seismic data, consequently their prediction and distributions are estimated statistically. Sub-seismic faults could potentially impact on productivity and consideration is given to their presence in some modeling scenarios. Due to the complexity of building a topologically consistent structural model only the largest faults (≥ 20m) were taken into Petrel. Some of the smaller faults were modeled as transmissibility barriers on cell boundaries in the dynamic modeling, depending on the fault seal scenario used.

Chinguetti-1 tested three stacked Tertiary reservoir fairways (pools A, B C), encountering hydrocarbons in the A and B reservoirs. The C sand penetrated in the well is interpreted to be water bearing.

Petrophysics Chinguetti-1 tested three stacked Tertiary reservoir Target fairways (A, B and C sands) developed over the faulted crest and flanks of the Khede Prospect (Chinguetti field). The B sands contained a 7metre gross gas column with a Gas Water Contact (GWC) at 1992 mRT. Average porosity in the B sand was 27%. The A sands contained an oil column in good quality sands. 31 meters of net sand with an average porosity of 26% was intersected. Oil saturation in the good quality sands ranged up to 90%. An Oil Up To (OUT) of 2414.9 mRT and an Oil Down To (ODT) of 2531 mRT were intersected. Preliminary petrophysical analysis identified the C sands as water bearing, with an average porosity of 30%. All oil-bearing sands encountered were in pressure communication.

Therefore, this study aims to integrate 3D seismic (SEG-Y) and well data (LAS, ASCII, TXT formats) to systematically characterize salt-related structural styles impact on reservoir compartmentalization, while evaluating reservoir quality within the field and assessing the mineralogical composition of these targets (SWC core samples); the results can be used to appraise and benchmark analogous Miocene fields such as Banda, TEVET, and Tiof within the MSGBC Basin.

GEOLOGY SETTING

The NW African margin of the Central Atlantic has two major salt basins, the Moroccan and the Mauritanian which form part of the MSGBC basin, and contain the Central Atlantic Magmatic Province (Fig. 2) (Tari et al., 2003; Davison, 2005; Vear, 2005; Dahmane et al., 2025; Ndiaye, 2012). The Chinguetti field is located within Block 4, PSC B, some 80 km offshore of Mauritania, in water depth of 800 m. The field structure is a faulted anticline, with Miocene-aged channelized turbidity sediments draped over an underlying salt diapir (Afifi et al., 2021). The field was discovered in May 2001 (Chinguetti-1 Well Proposal, 2001).

The reservoir section in the Chinguetti field is subdivided into three main packages based on Calcareous Nannoplankton (CN) age dating and are referred to as the CN1, confined to the base of the Chinguetti canyon; CN2, upper canyon confined to partially unconfined sediments; and CN3 sediments, which represents the spill phase of the canyon fill (Chinguetti-4-2 Well Completion Report, 2002).

The reservoir depths are between 2200–2800 m TVDss, with initial reservoir pressure of 3500–4200 Psig (Bah, 2026). Furthermore, the structure is a faulted domal anticline developed over the crest and flanks of a Miocene salt-cored diapir (Tari et al., 2003; Tari and Jabour, 2013).

Salt tectonics framework in the Chinguetti field shows strong analogues with the Dead Sea, Gulf of Mexico, and Campos basins, characterized by similar fault–fracture patterns, migration pathways, and compartmentalization, confirming a consistent and predictive structural framework across salt-controlled systems (Tari and Jabour, 2013; Alsop et al., 2018; Afifi et al., 2021).

Early Jurassic evaporites are interpreted to have developed in a restricted basin located within blocks 2–6 in Mauritania. It appears that this salt basin was relatively restricted and probably only contained a small volume of salt compared to the more substantial basins of northern Angola and the Gulf of Mexico (Davison, 2005; Vear, 2005).

This salt basin is interpreted to be of a similar age and size to the Tafraya Basin in central Morocco. In Mauritania, a rapid Valanginian transgression and subsequent clastic deposition of the Barremian terminated the development of the carbonate bank. The post-Valanginian stratigraphy of Mauritania is dominated by several third-order cycles of clastic deposition punctuated by transgressive carbonates on the shelf (Davison, 2005; Ndiaye, 2012; Ndiaye et al., 2016).

These major transgressive events are associated with source rock deposition (transgressive and early highstand) in the Cenomanian–Turonian, Paleocene and possibly during the Late Aptian to Early Albian. The major lowstand events in the basin are associated with turbidity deposition in the Mid-Cenomanian, Late Maastrichtian, Middle Miocene and Late Miocene. These are typically either unconstrained fairways or confined by canyon development. The deepwater is otherwise shale-prone as indicated by the offset wells (Davison, 2005; Vear, 2005; Ndiaye et al., 2016).

Furthermore, thermal subsidence in the basin has prevailed from Late Cretaceous to present day, interrupted by several compressional tectonic activities as a product of North African Plate movement. A conjugate ENE–WSW right-lateral and NW–SE left-lateral strike-slip fault system, affecting the Jurassic and Cretaceous rocks of northeastern Morocco to the Nouakchott compartment, was a product of this compressional tectonic activity from the Late Cretaceous to Paleocene, with maximum compression oriented E–W and ESE–WNW (Tari et al., 2012; Ndiaye et al., 2016).

Another stress tensor (conjugate system), denoted by E–W maximum compression, was observed in the Central High Atlas and coastal Atlantic basin areas, including offshore Rabat–Salé. This tectonic event occurred from the Late Cretaceous to Paleocene (Tari et al., 2012; Ndiaye et al., 2016).

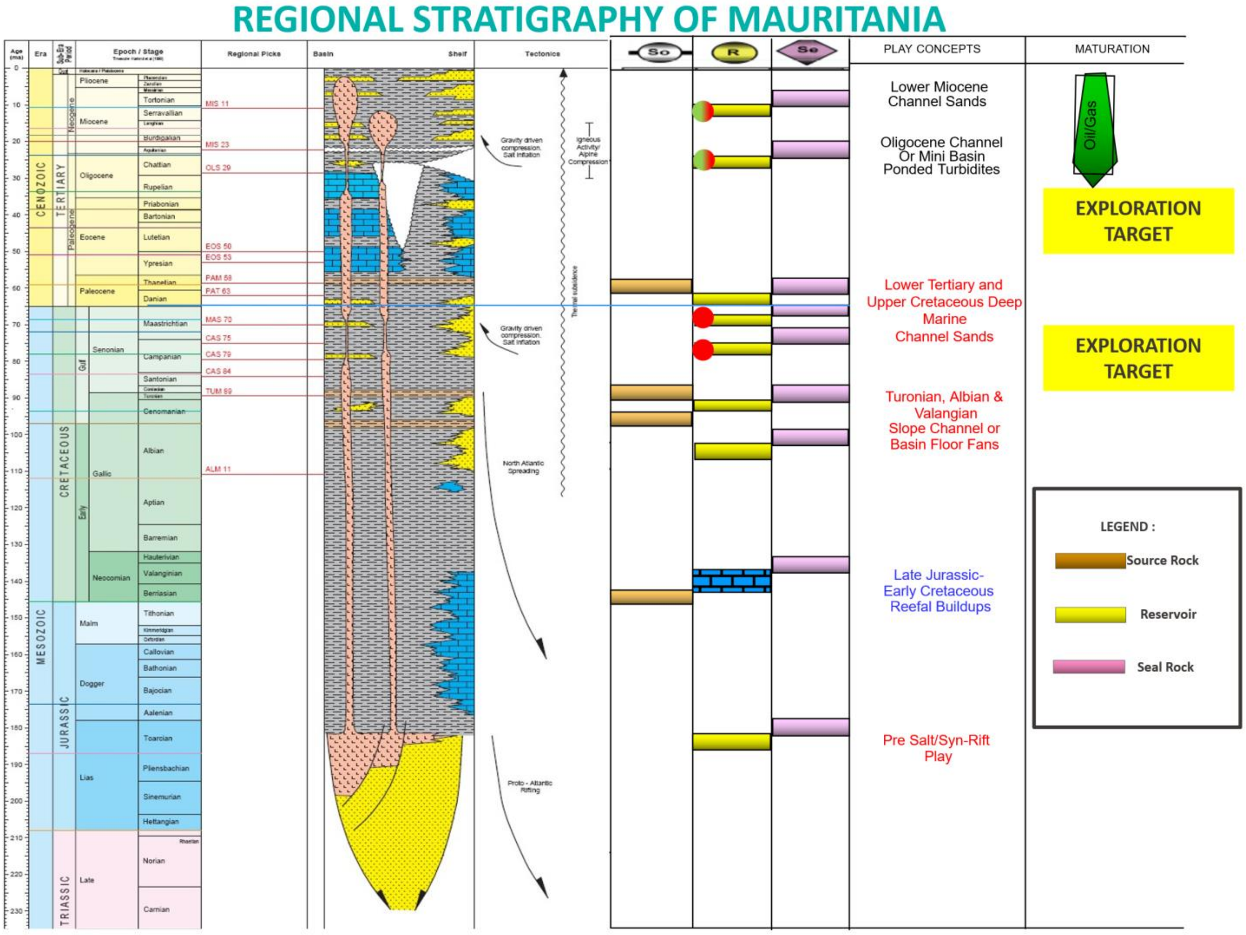

Fig.2. Post-Cenomanian Stratigraphic Framework of offshore Mauritania (Woodside, 2004).

By Eocene times, the changing stress elements of north-east Morocco and the Rif foreland indicate that the maximum compression was oriented N–S, and was resolved by NW–SE and NNE–SSW sinistral strike-slip faults, and E–ENE thrust faults (Tari et al., 2012).

At the Chinguetti field, the maximum horizontal stress orientation is interpreted as radial, essentially isotropic, but with a slight anisotropy in approximately the ENE–WSW direction (Dahmane et al., 2025).

Moreover, the primary charge source rock in the Mauritania 3D area is considered to be of Cenomanian–Turonian age (Davison, 2005; Vear, 2005).

The mature Turonian source kitchen extends from V-1 in the north to MTO-2 in the south, and accounts for oil at V-1 and oil shows in MTO-1, -2 and -3. It is identifiable on the Mauritanian 3D Survey as a parallel seismic facies bounded by two mappable flooding surfaces of Turonian and Santonian age (Vear, 2005; Chinguetti-1 Well Proposal, 2001).

The interval thins to the southern part of the 3D survey onto the ‘Shafr al Khanjar’ High, and eastwards onto a hinge zone developed over the edge of the Neocomian carbonate bank. Three-dimensional basin modeling predicted the Turonian to be peak to late peak oil mature across the Khede Prospect and locally gas mature in salt withdrawal synclines. The dominant hydrocarbon product was expected to be oil and minor gas (Chinguetti-1 Well Proposal, 2001; Vear, 2005).

The Chinguetti-1 oil is a low-maturity, 30° API, paraffinic, low-sulphur crude oil with a moderate pour point. Maturity parameters suggest the oils were expelled below peak maturity

(c. 0.65–0.75% Ro Vit). The relatively low API gravity is a function of maturity and not biodegradation (Pogson, 2003). Vertical migration along the salt weld beneath Chinguetti-1 is likely to be the primary liquid hydrocarbon migration conduit between source and reservoir (Dahmane et al., 2025; Tari et al., 2003).

METHODOLOGY AND DATA

The PreSTM data used for Khede Prospect mapping were processed by VERITAS and Woodside's in-house Geophysics Team, which delivered earlier fast-track post-stack time migration (PostSTM) sub-volumes during Q2–Q3 2000 (Chinguetti-1 Well Proposal, 2001).
The data were 'binned' to 25 m × 25 m to achieve 46-fold. Data quality was considered good. The PETREL Software 2018 from Schlumberger Company was used to plot the seismic sections and interpretations of traps as salt domes, faults and horizons, and well-log data (LAS, ASCII and TXT files) were plotted using TECHLOG 2018. Well logs including GR, Sonic, Neutron, RES and HC Sat were used to identify hydrocarbon-bearing zones (Sturrock, 2003; Slade, 2005).
A total of 63 samples [4 core and 59 DC samples] from the interval 1730 m to 2655 m in Chinguetti-4-2 and 1 have been examined for calcareous nannoplankton on the well site (Chinguetti-4-2 Well Completion Report, 2002). Cores were logged in digital format using AppleCoreTM. Colours were determined by comparing the wet core face with the Geological Society of America (GSA) color chart (Chinguetti-4-2 Well Completion Report, 2002). Cores were logged in digital format using AppleCoreTM. Colours were determined by comparing the wet core face with the GSA color chart.
The petrophysical parameters interpreted in this study were obtained from data processed by Core Laboratories (Sturrock, 2003; Slade, 2005).

Lithology

Shale volume, VSH, was calculated from the gamma-ray log using a linear transformation (Aliouane, 2022):

$$\boldsymbol{VSH} = \frac{\boldsymbol{GR - GRclean}}{\boldsymbol{GRshale - GRclean}} \quad (1)$$

A density-log cutoff, consistent with the one previously applied in the field, was applied to determine the tight zones (Sturrock, 2003; Slade, 2005).
Porosity, DPHI, was calculated using the density curve over the A-sand interval (Sturrock, 2003):

$$\boldsymbol{DPHI} = \frac{(\boldsymbol{RHOG - RHOB})}{(\boldsymbol{RHOG - RHOF})} \quad (2)$$

Gas corrected:

$$porosity = (\boldsymbol{3 * DPHI + 2 * NEUTRON}) / \boldsymbol{5} \quad (3)$$

where DPHI is defined above, and NEUTRON is sandstone neutron porosity values (CNCF/100 + 04).
Saturations were calculated using the Archie equation (Sturrock, 2003; Ahmed and Farman, 2023):

$$\boldsymbol{Swn} = (\boldsymbol{a/\emptyset m}) \left(\frac{\boldsymbol{Rw}}{\boldsymbol{Rt}}\right) \quad (4)$$

NET TO GROSS Net reservoir in this analysis was defined using the cutoffs:
$VSH\ 0.15, DT > 350\ usec/m$
To obtain good-quality data for the determination of reservoir sequences, lithofacies and rock properties through core and log analysis, particularly in the northern fan complex (Chinguetti-1 Well Proposal, 2001; Sturrock, 2003).
A total of twenty-four percussion (SWC) and rotary (MSCT) sidewall core samples were submitted for petrographic analysis from the Chinguetti-1 well (Chinguetti-1 Well Proposal, 2001).

The analyses were specified by Woodside Energy Ltd. and included detailed thin-section description and modal point counting (up to 250 points), Scanning Electron Microscopy (SEM), X-Ray Diffraction (XRD), and thin-section grain-size analyses. Only three zones of interest in the Chinguetti-1 well were investigated, at depths of 2430–2442 m, 2445–2462.5 m, and 2522–2531.5 m. The analytical workflow was carried out by Core Laboratories (Sturrock, 2003).

Furthermore, thin-section petrography was performed on samples provided as sidewall cores, which were impregnated with blue-dyed epoxy and mounted on oversized, covered petrographic slides. Thin-section petrographic analysis was conducted using a Zeiss petrographic microscope, and representative thin-section photomicrographs were taken at two magnifications for each sample (40× and 100×). Whole-thin-section photomicrographs were also taken of each sample at 8× (Sturrock, 2003).

RESULTS AND DISCUSSIONS

The Chinguetti field highlights the presence of a high net-to-gross oil and gas reservoir compartmentalized into several levels, with different porosity and permeability characteristics based on the structural, petrographic and petrophysical signatures observed in the field (Dahmane et al., 2025; Sturrock, 2003). The reservoir is intersected by three main levels, A, B and C, with Level A representing a high-NTG oil-bearing level, whereas Level C has very low NTG and is water-bearing (Dahmane et al., 2025; Sturrock, 2003).

The primary petrophysical uncertainty in the field is considered to be permeability (Sturrock, 2003; Hosseini et al., 2019). An uncertainty factor of ± a factor of two is quoted in the original derivation of the grain-size model. The main channel sands observed in the wells do not appear to contain internal shale bands, which supports the mid-case assumption that they are not highly stratified, and the thin sands are modelled separately.

However, the effects of internal and basal shale drapes and similar vertical permeability barriers are not well known or adequately modelled to date, especially for the thinly bedded levee and overbank lithofacies (Dahmane et al., 2025).

Structural setting in the field:

From the seismic section (Fig. 3), the Chinguetti field appears to be highly faulted. Salt diapirism and associated uplift generated a structurally complex, folded crest characterized by intense faulting and fracturing, producing pronounced structural anisotropy and heterogeneity in reservoir connectivity across the field (Tari et al., 2003; Alsop et al., 2018; Dahmane et al., 2025).

The field is a faulted salt anticline, with Miocene-aged channelized turbiditic sediments draped over an underlying salt diapir (Afifi et al., 2021; Tari and Jabour, 2013; Dahmane et al., 2025).

The Chinguetti reservoirs were deposited between 23 and 15 Ma, representing the Early and Middle Miocene epochs. The reservoir represents mid-slope and canyon-fill sediments, comprising turbiditic sandstones, siltstones, and mudstones, which were originally deflected around the seafloor expression of the Chinguetti salt diapir within a large regional seafloor canyon before backfilling and spilling over a width of up to 7 km (Vear, 2005; Dahmane et al., 2025).

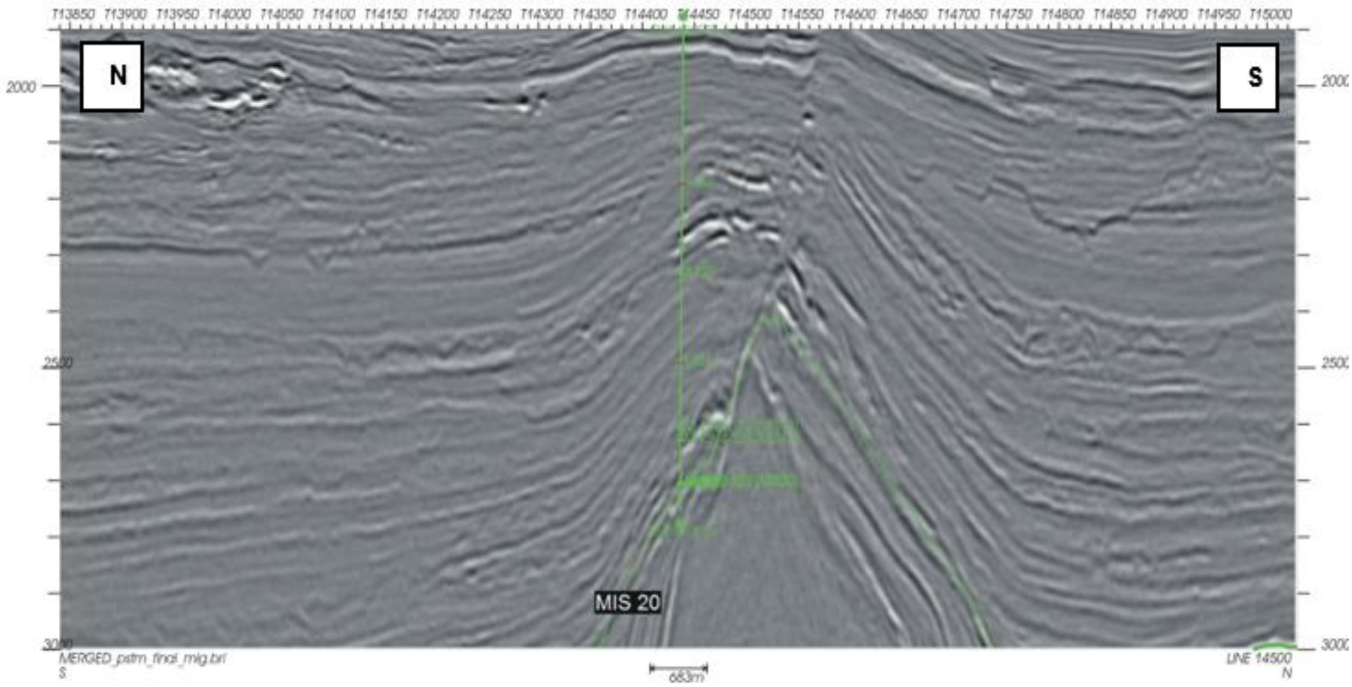

Fig.3. Chinguetti -1 well seismic section through MIS 20.

The reservoir section in the Chinguetti field is subdivided into three main packages based on Calcareous Nannoplankton (CN) age dating, referred to as CN1, confined to the base of the Chinguetti Canyon; CN2, representing the upper canyon and comprising partially unconfined sediments; and CN3, representing the spill phase of the canyon fill (Chinguetti-4-2 Well Completion Report, 2002).

The CN1 stacked channel sands have only been encountered on the southern flank of the Chinguetti field as well as in the Banda field (Chinguetti-4-2 Well Completion Report, 2002; Dahmane et al., 2025).

As shown in Fig. 4, the field is divided into three main structural compartments with different GOC and OWC contacts. The dominant east–west-trending fault dividing the upthrown northern block from the southern blocks is thought to have formed in response to the growth of the larger Corvina salt diapir a few kilometers to the northwest (Dahmane et al., 2025; Tari et al., 2003).

This main fault appears to have been reactivated, with a shallow overburden expression as well as numerous overburden antithetic faults associated with it. This large fault overprints smaller faults, which appear to have a radial component related to the original intrusion of the salt diapir and the formation of the Chinguetti dome (Alsop et al., 2018; Dahmane et al., 2025). A large north–south radial fault further subdivides the southern block into SE and SW blocks (Dahmane et al., 2025).

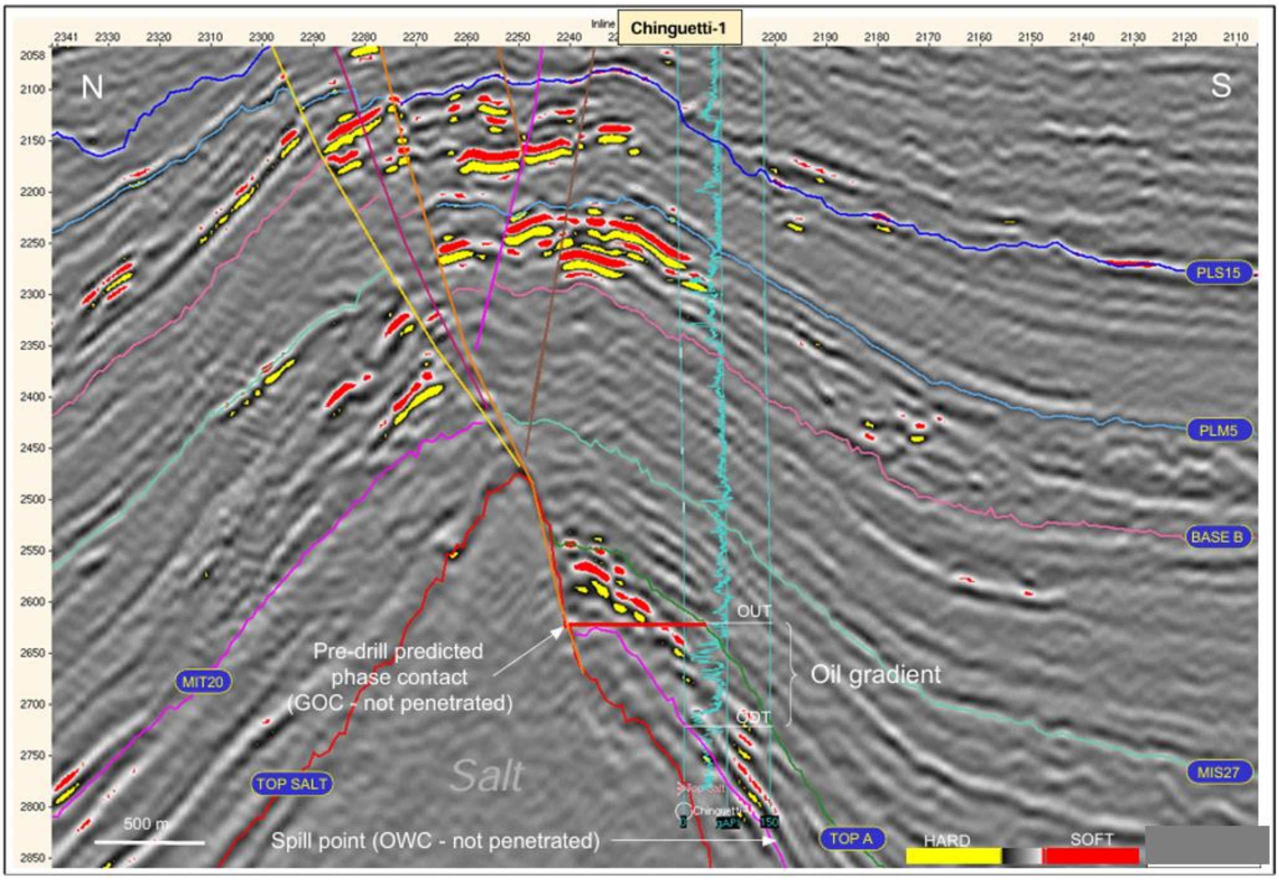

Fig.4. Chinguetti-1 Seismic Cross-section.

Post-drill remapping indicates that the structural model is broadly unchanged (Fig. 5). The main remaining uncertainty in future structural mapping is the effect of minor sub-radial faults associated with the main fault on reservoir connectivity and the precise position of structural spill points for each fault block (Dahmane et al., 2025; Dahmane et al., 2026b).

The maximum throw at Top A level on the main fault is approximately 300 m. Post-well remapping and careful placement of fault traces indicate possible communication between upthrown and downthrown blocks. Further detailed mapping and fault-plane interpretation should form part of the appraisal and development feasibility studies (Dahmane et al., 2025; Dahmane et al., 2026b).

Understanding this compartmentalization will provide greater certainty regarding lateral connectivity when exploiting the same Miocene reservoir fields (Banda, Tevet, and Tiof) (Société Mauritanienne des Hydrocarbures, 2024; Dahmane et al., 2025; Dahmane, 2026; Dahmane et al., 2026b). These fields contain significant hydrocarbon resources in the same coastal basin and could potentially be developed based on a better understanding of the structural and reservoir connectivity. The fields were initially considered in the context of the Chinguetti discovery but subsequently faced development challenges associated with compartmentalization, pressure depletion, production decline, and connectivity uncertainty (Dahmane, 2026; Dahmane et al., 2026b).

It is important to note that the results from the 3D seismic sections (Figs. 4 and 5) are consistent with observations from post-salt reservoirs in the Campos Basin (Brazilian margin), where comparable reservoir compartmentalization and trap development have been documented, with salt folds typically trending from NNE–SSW to NE–SW, subparallel to the salt walls in the coastal basin (De Jesus and Cardoso Vilela, 2023).

Natural fractures form two principal conjugate sets with a consistent NNW–SSE strike orientation. One set dips toward the SW, whereas the second set dips toward the NE to E (Dahmane et al., 2025; Willis et al., 2006; Bagheri and Mohebian, 2025).

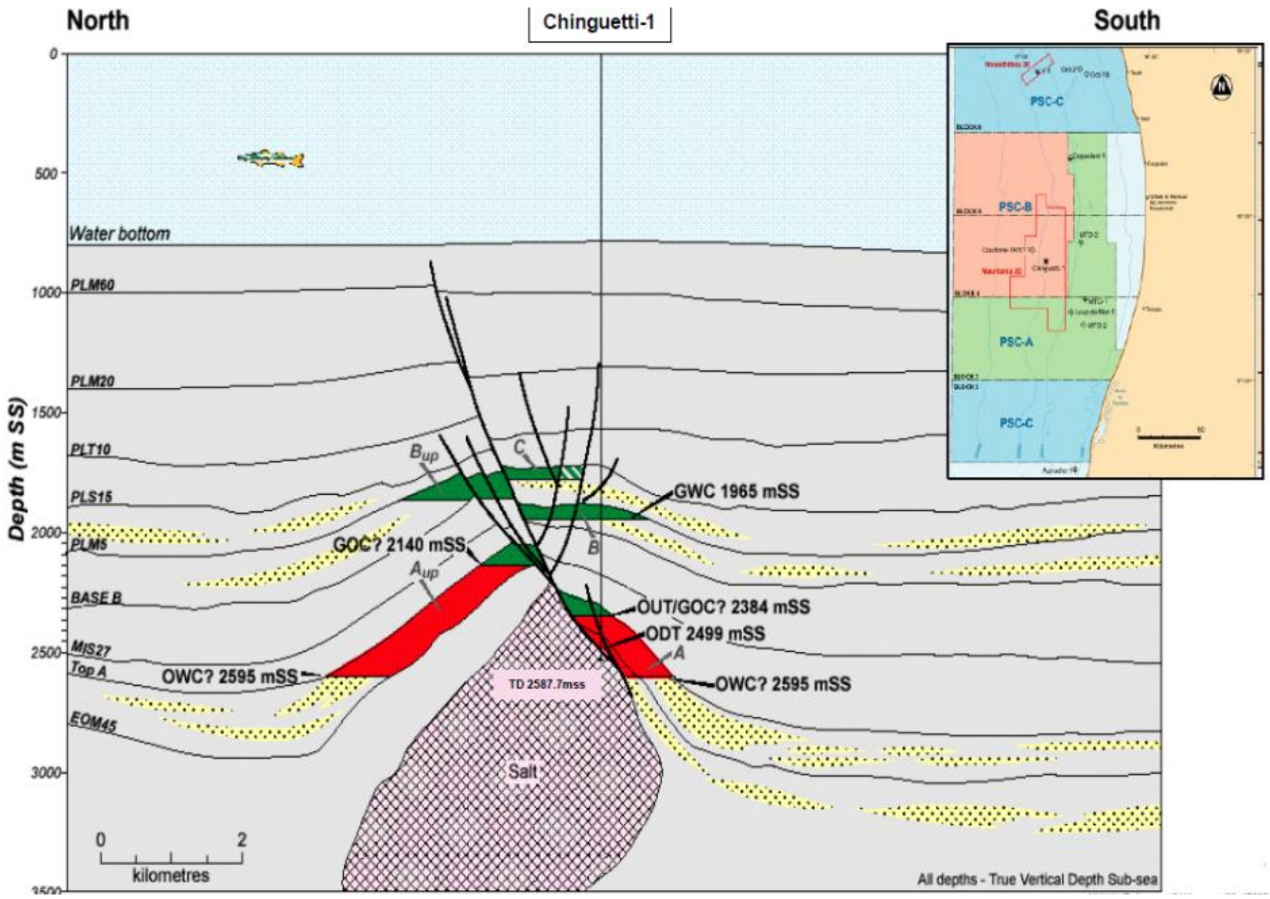

Fig.5. Chinguetti Geoseismic– Postdrill reservoir seismic section (Dahmane et al., 2025).

Petrography and petro physics

Three zones of interest in the Chinguetti-1 well are identified from log depths of 2430 to 2442 m, 2445 to 2462.5 m, and 2522 to 2531.5 m (Fig. 6, Fig. 7) (Chinguetti-1 Well Proposal, 2001; Sturrock, 2003). The zones are discussed below in terms of reservoir rock types, estimated petrophysical properties, and log response. Thin-section photomicrographs of the samples are provided in Plates A to F (Fig. 8) (Sturrock, 2003).

The net-to-gross ratio (N:G) of the main reservoir interval was 24%, and the average log-derived porosity was 24% (Sturrock, 2003). The oil-down-to (ODT) is interpreted at 2453.5 mRT, with a possible free-water level (FWL) interpreted at 2478 mRT (Chinguetti-1 Well Proposal, 2001; Sturrock, 2003). Although the exact depth of the FWL is subject to some uncertainty, it was encountered shallower than expected. Together with the absence of a common gas-water contact with Chinguetti-1, this observation indicated the presence of north–south compartmentalization within the field (Chinguetti-1 Well Proposal, 2001; Dahmane et al., 2025).

A large-format montage of thin-section petrography and rock-type data is presented in the accompanying panel.

Petrological studies and rock typing have been carried out on sidewall cores and rotary sidewall cores from the reservoir intervals identified from petrophysical logs, including gamma ray (GR), porosity-neutron (PoroNeut), resistivity, and hydrocarbon-saturation logs

(Sturrock, 2003; Slade, 2005). Three zones of interest representing reservoir levels are discussed below.

Zone of Interest: 2430 to 2442 m (Sand C)

This zone consists of an overall fining-upward succession, with 1–2 m thick sands at the base (Fig. 7) (Chinguetti-1 Well Proposal, 2001; Sturrock, 2003). The sample from this zone was collected at 2434 m. The sample is a slightly consolidated, clay-laminated sandy mudstone (Plates A and B) and is not representative of the thin sands within the zone of interest (Sturrock, 2003).
The silt- and sand-sized material is composed mainly of quartz, with minor feldspar (Plates A and B). Sandstone samples have undergone only minor compaction. This low degree of compaction is evidenced by the predominance of point contacts over planar grain contacts. The sample contains no significant interconnected porosity and is therefore considered non-reservoir rock (Sturrock, 2003). Consequently, this interval is not considered further in the reservoir analysis.

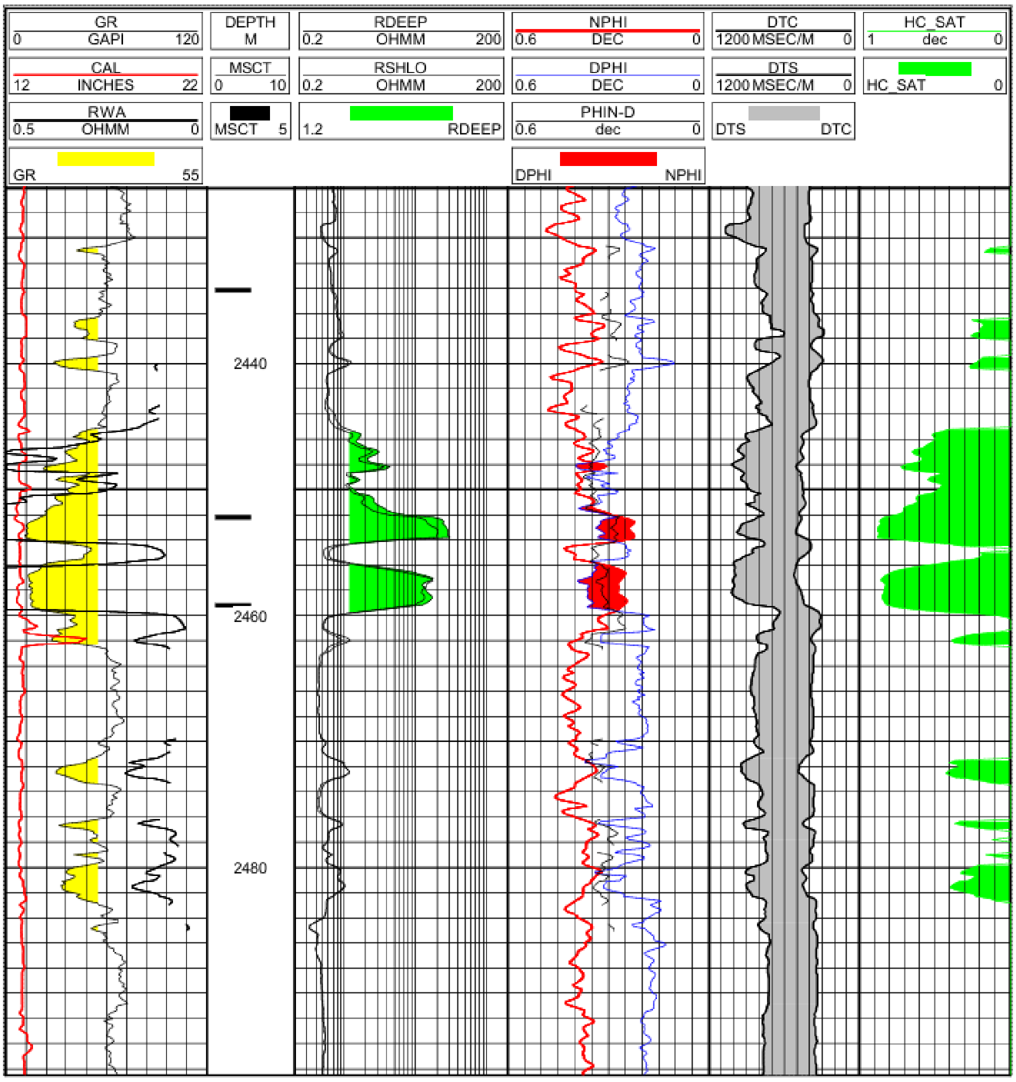

Fig.6. Chinguetti-1 Petrophysics Log 2400m to 2500m.

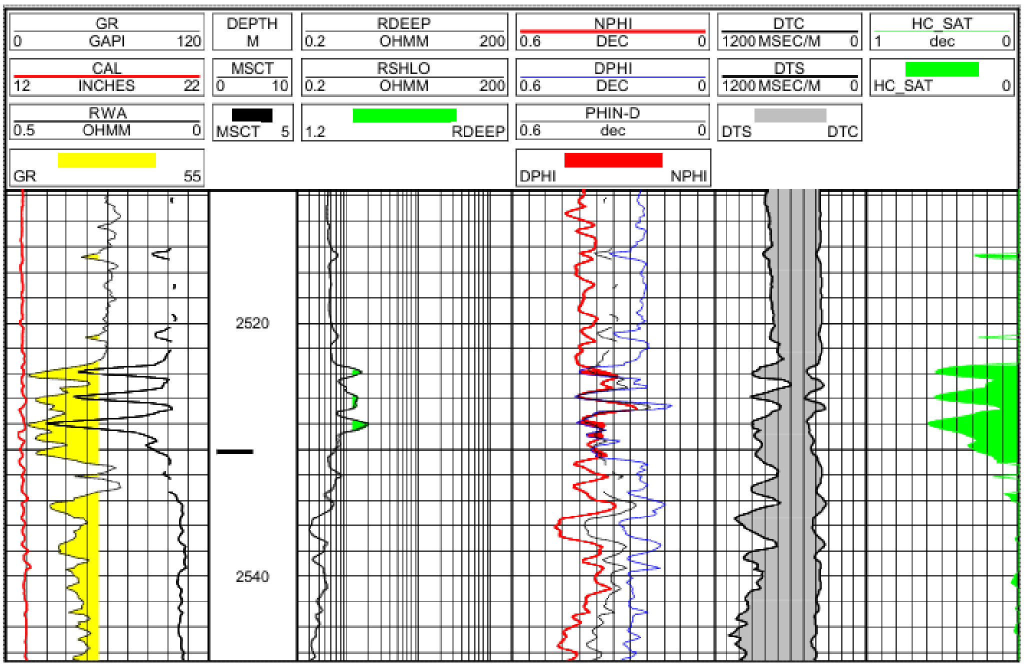

Fig.7. Chinguetti-1 Petrophysical log 2500 to 2550 m.

Zone of Interest 2445 to 2462.5 meters (Sand B)

This zone consists of an overall fining-upward sequence, containing sets of approximately 4 m thick sands (Fig. 6) (Sturrock, 2003). There are two samples from this interval, located at 2452 and 2459 m. Both samples are unconsolidated, moderately sorted, lower-medium-grained sands composed of quartz, minor feldspar, and traces of carbonate detritus (Fig. 8; Plates C and D) (Sturrock, 2003).

Traces of clay and zeolite at 2452 m are the only cements present. The estimated clay content is less than 2.5%, and the estimated porosity is 30–35% (Sturrock, 2003). An analogue for these thick sands has a porosity of 32%, a permeability of 2520 mD, and an effective permeability to gas of 1570 mD at an irreducible water saturation of 13% (Sturrock, 2003). The Archie cementation (*m*) and saturation (*n*) exponents are 1.61 and 1.92, respectively (Sturrock, 2003).

The gamma-ray log response for the sample at 2452 m is 20–24 API, with a deep resistivity reading of 5–18 ohm·m and density-derived porosity of 27–33% (Fig. 8) (Sturrock, 2003; Slade, 2005).

The neutron porosity is 26–30%, showing a symmetrical crossover with the density log. A gas-corrected (Gaymard and Poupon, 1968) density-neutron porosity ranges from 27–32% (Sturrock, 2003). The shear velocity is relatively low, ranging from 765 to 805 µs/m. The interval has five calculated hydrocarbon saturation values ranging from 80–88% (Sturrock, 2003).

The log response at the sampled depth of 2459 m shows gamma-ray values of 15–16 API, a deep resistivity of 14–17 ohm·m, and density-derived porosity of 34–36% (Fig. 8) (Sturrock, 2003; Slade, 2005). Neutron porosity ranges from 24–26%, with a fair symmetrical crossover. A gas-corrected (Gaymard and Poupon, 1968) density-neutron porosity ranges from 30–32% (Sturrock, 2003). The shear velocity ranges from 830 to 960 µs/m. The calculated hydrocarbon saturation for this interval ranges from 84–85% (Sturrock, 2003).

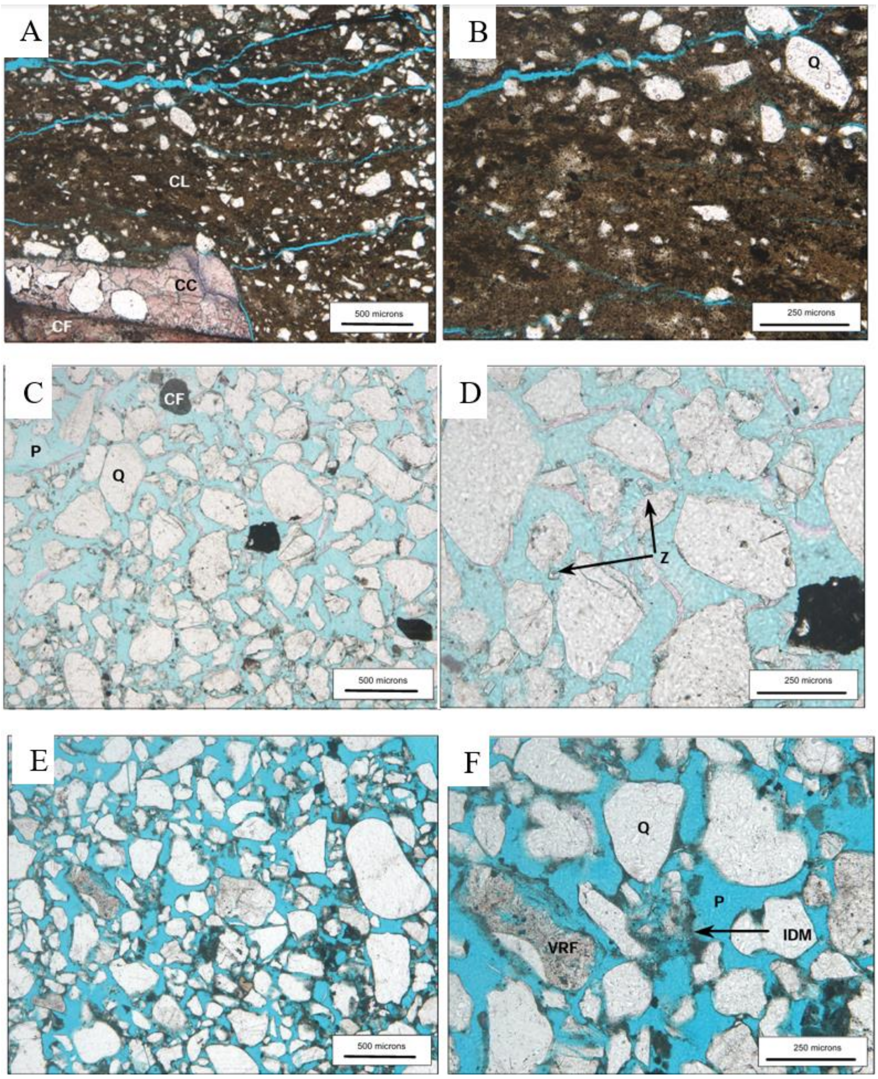

Fig.8. Whole Thin Section Photograph; (A C E - 43X; B D F - 110X).

Plates A and B: This sample is a very porous, unconsolidated, moderately sorted, medium-grained sand displaying a massive fabric. The dark spots are carbonate detritus and, in part, drilling or preparation contaminants. Porosity (blue) is abundant and well interconnected. The gap in the black bar at the bottom of the photograph is 1 mm wide for reference. 8× (Sturrock, 2003).

Plates C and D: This sample is an unconsolidated, moderately sorted, medium-grained sand. The sample fragments contain dark contaminants from the coring process. The sample contains only traces of clay. Porosity is abundant and well interconnected. The gap in the black bar at the bottom of the photograph is 1 mm wide for reference. 8× (Sturrock, 2003).

Plates E and F: This sample is an unconsolidated, well-sorted, upper-fine-grained sand that displays a massive fabric. Minor amounts of zeolite and cristobalite are the dominant cementing agents. Porosity is abundant and well interconnected. The gap in the black bar at the bottom of the photograph is 1 mm wide for reference. 8× (Sturrock, 2003).

Zone of Interest 2522 to 2531.5 meters (Sand A)

The interval has a serrated gamma-ray log pattern over an 8 m gross sand interval (Fig. 7) (Sturrock, 2003). The sample from this interval is from 2530 m. The sample is an unconsolidated, well-sorted, upper-fine-grained sand composed of quartz and minor feldspar. The sand is clean, with an estimated clay content of less than 2.5% and an estimated porosity of 30–35%. The principal cements are zeolite and cristobalite (Sturrock, 2003).

This sand classifies as a 42112:9 rock type. An analogue for this sand has a porosity of 35%, a permeability of 1300 mD, and an effective permeability to gas of 1250 mD at an irreducible water saturation of 9%. Analogue Archie parameters, *m* and *n*, are 1.86 and 2.06, respectively (Sturrock, 2003).

The gamma-ray log response for this interval is 17–19 API, the deep resistivity response is 0.6–0.7 ohm·m, and the density-derived porosity is 35–36%. The neutron porosity ranges from 32–34%. A gas-corrected (Gaymard and Poupon, 1968) density-neutron porosity is 34–35%. The shear velocity ranges from 860 to 880 µs/m. Calculated hydrocarbon saturation at this sample depth is approximately 30%. Immediately above the sample, similar sands in this zone have calculated hydrocarbon saturations between 50% and 60% (Sturrock, 2003; Slade, 2005).

The log pattern indicates that this sample is below or at the hydrocarbon-water contact (Sturrock, 2003). However, traces of dissolution porosity are observed in some feldspars and a few zeolite crystals (Plates E and F). At least in the zeolite, this dissolution is likely to have been a relatively late event. However, some of the dissolution porosity observed in feldspars could have been inherited, possibly due to weathering prior to deposition (Sturrock, 2003).

The main control on porosity and permeability is the presence or absence of detrital clay matrix (Sturrock, 2003). In relatively clean sandstones, such as those at 2459.0 m and 2530.0 m, permeability has been reduced by the presence of microporous cristobalite (Sturrock, 2003; Chen et al., 2024). The sandstone at 2530.0 m exhibits very high core-analysis porosity (helium porosity of 32.4%) but only moderate permeability (Klinkenberg permeability of 174 mD) (Fig. 9) (Sturrock, 2003).

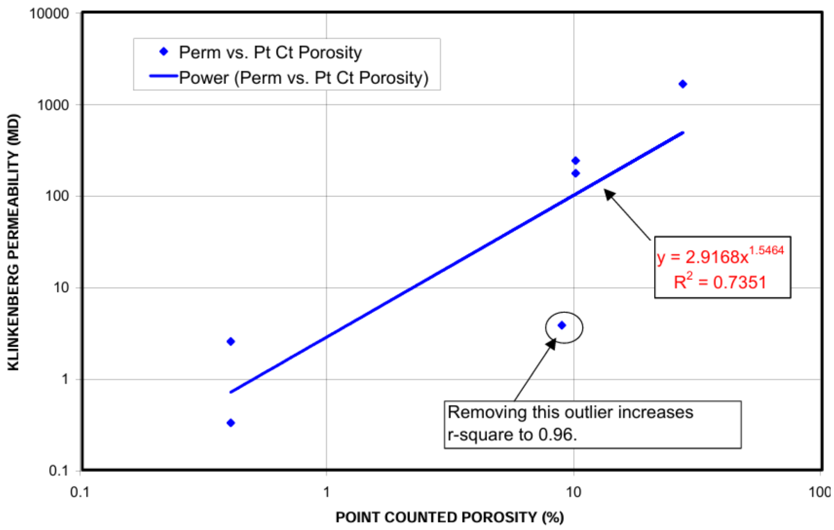

Fig.9. Permeability Vs. Point Counted Porosity, Chinguetti-1.

The very high porosity of this sample is due to the high microporosity associated with pore-filling cristobalite, while the grain-coating and pore-filling habits of this cristobalite have acted to reduce permeability (Sturrock, 2003; Chen et al., 2024). Another important control, mainly affecting permeability, is grain size. The best-quality sandstones in the sequence are also the coarsest-grained (2452.0 m, 2459.0 m, 2524.0 m, 2528.0 m, and 2530.0 m; Fig. 8 and Plates A, B, E and F) (Sturrock, 2003). Point-counted values of visible porosity correlate very well with Klinkenberg permeability when plotted logarithmically (Fig. 9) (Sturrock, 2003).

CONCLUSIONS

From the present study of the highly compartmentalized reservoir of the Chinguetti field in the offshore MSGBC Basin of Mauritania, the following conclusions can be drawn:

Seismic sections indicate that salt uplift has generated numerous faults and fractures, rendering the reservoirs significantly more complex and compartmentalized than initially anticipated (Tari et al., 2003; Alsop et al., 2018; Dahmane et al., 2025). Moreover, heterogeneous fluid contacts and compartmentalization contribute to the structural and fluid-flow complexity of the field (Dahmane et al., 2025; Dahmane et al., 2026b).

Petrophysical logs for the Chinguetti field indicate high reservoir quality, with permeability of around 150 mD and a thick net-to-gross reservoir interval (Sturrock, 2003). The studied interval shows five calculated hydrocarbon saturations ranging from 80% to 88% (Sturrock, 2003). Analogue data for these thick sands suggest a porosity of 32%, permeability of 2520 mD, and an effective gas permeability of 1570 mD at an irreducible water saturation of 13% (Sturrock, 2003).

The corresponding Archie parameters (m = 1.86 and n = 2.06) further support favorable reservoir characteristics (Sturrock, 2003). Log responses are consistent with clean, high-quality sands, with gamma-ray values between 17 and 19 API, deep resistivity ranging from 0.6 to 0.7 ohm·m, and density-derived porosity between 35% and 36% (Sturrock, 2003). These characteristics indicate excellent reservoir properties within the studied interval.

Petrographic and mineralogical analyses indicate a quartz-dominated, well-sorted, fine-grained sandstone with minor feldspar and negligible clay matrix (<2.5%), reflecting a clean framework and well-preserved primary intergranular porosity (Sturrock, 2003). Diagenesis is primarily controlled by pore-filling and grain-coating cristobalite and subordinate zeolite cement, generating significant microporosity while partially occluding pore throats (Sturrock, 2003; Chen et al., 2024). Secondary dissolution features affecting feldspar and zeolite locally enhance pore development (Sturrock, 2003). Overall, the reservoir exhibits excellent porosity governed by depositional texture and diagenetic overprint, whereas permeability is moderated by silica cementation and microporous phases (Sturrock, 2003; Chen et al., 2024).

REFERENCES

Ahmed, R., Farman, G. M. (2023). How to estimate the major petrophysical properties: A review. *Iraqi Journal of Oil and Gas Research*, *3*(1), 43–58. https://doi.org/10.55699/ijogr.2023.0301.1037

Afifi, A., Heyn, T., William, C., Da Silva, E. (2021). Polyphase faulting and raft tectonics in Sureste Basin offshore Mexico. *Third EAGE Conference on Offshore Exploration and Development in Mexico*, European Association of Geoscientists and Engineers, 1–2. https://doi.org/10.3997/2214-4609.202184011

Aliouane, L. (2022). Levenberg-Marquardt algorithm neural network for clay volume estimation from well-log data in an unconventional tight sand gas reservoir of Ahnet Basin (Algerian Sahara). *Bulletin of Geophysics and Oceanography, 63*, 443–454. https://doi.org/10.4430/bgo00391

Aliouane, L., Ouadfeul, S.-A., Djarfour, N., Boudella, A. (2012). Petrophysical parameters estimation from well logs data using multilayer perceptron and radial basis function neural networks. In T. Huang, Z. Zeng, C. Li, C. S. Leung (Eds.), *Neural Information Processing, ICONIP 2012* (Lecture Notes in Computer Science, Vol. 7667, pp. 730–736). Springer, Berlin, Heidelberg. https://doi.org/10.1007/978-3-642-34500-5_86

Alsop, G. I., Weinberger, R., Marco, S., Levi, T. (2018). Fault and fracture patterns around a strike-slip influenced salt wall. *Journal of Structural Geology, 106*, 103–124. https://doi.org/10.1016/j.jsg.2017.10.010

Bah, D. (2026). Integrated geological, stratigraphic, geochemical, and petrophysical characterization of offshore Block 7, Mauritanian Coastal Basin: Pelican Field. *Second*

EAGE Workshop on Advances in Carbonate Reservoirs: From Prospects to Development, 1–3. https://doi.org/10.3997/2214-4609.2026649063

Bagheri, B., Mohebian, R. (2025). Fracture facies estimation utilizing machine learning algorithm and Formation Micro-Imager (FMI) log. *Petroleum Research*. https://doi.org/10.1016/j.ptlrs.2025.04.006

Bian, Q., Shang, D., Lin, H., Han, J. (2022). Strike-slip salt tectonics in the Shuntuoguole Low Uplift, Tarim Basin, and the significance to petroleum exploration. *Marine and Petroleum Geology*, *139*, 105600. https://doi.org/10.1016/j.marpetgeo.2022.105600

Chen, G., Ba, J., Zhu, H., Carcione, J. M., Gao, L. (2024). The effect of pore structure on the permeability of tight sandstones. *Bulletin of Geophysics and Oceanography, 65*(4), 593–610. https://doi.org/10.4430/bgo00471

Chinguetti-1 (Khede Prospect) Well Proposal. (2001, March). WEL. Unpublished results.

Chinguetti-4-2 Well Completion Report, Basic Data, Rev. 1. (2002, April). WEL. Unpublished results.

Dahmane, B. (2026). Chinguetti Field failure versus the Banda, TEVET, and TIOF fields: Reservoir evaluation and economic performance. *87th EAGE Annual Conference and Exhibition*, 1–5. https://doi.org/10.3997/2214-4609.2026101627

Dahmane, B., Aliouane, L., Nabawy, B. S., Guareche, M. (2025). Integrated fractured reservoir modeling and secondary oil recovery techniques: A historical case study for productivity improvement in the Chinguetti offshore oil reservoir in the Coastal Basin of Mauritania. *Journal of Petroleum Geology*. https://doi.org/10.1111/jpg.70027

Dahmane, B., Aliouane, L., Rigane, A. (2026b). Reservoir failure and connectivity: The Chinguetti–Bir Allah analogue. In *First EAGE/ALNAFT Workshop – Unlocking Hydrocarbon Potential of West Mediterranean Offshore Frontier Basin of Algeria*, European Association of Geoscientists and Engineers (EAGE), 1–3. https://doi.org/10.3997/2214-4609.2026651036

Davison, I. (2005). Central Atlantic margin basins of northwest Africa: Geology and hydrocarbon potential (Morocco to Guinea). *Journal of African Earth Sciences, 43*(1–3), 254–274. https://doi.org/10.1016/j.jafrearsci.2005.07.018

De Jesus, A., Cardoso Vilela, P. (2023). Campos basin: Review on the geology and its oil and natural gas exploration and production context. *Latin American Journal of Energy Research*, *10*(1), 1–12. https://doi.org/10.21712/lajer.2023.v10.n1.p1-12

Gaymard, R., Poupon, A. (1968). Response of neutron and formation density logs in hydrocarbon bearing formations. *The Log Analyst*, *9*(5), 3–12. https://doi.org/10.3997/1365-2397.1985009

Hosseini, M., Riahi, M. A., Mohebian, R. (2019). A meta-attribute for reservoir permeability classification using well logs and 3D seismic data with probabilistic neural network. *Bollettino di Geofisica Teorica ed Applicata*, *60*(1), 81–96. https://doi.org/10.4430/bgta0257

Letouzey, J., Colletta, B., Vially, R., Chermette, J. C. (1995). Evolution of salt-related structures in compressional settings. In M. P. A. Jackson, D. G. Roberts, S. Snelson (Eds.), *Salt Tectonics: A Global Perspective* (AAPG Memoir 65, pp. 41–60). American Association of Petroleum Geologists.

Letouzey, J., Sherkati, S. (2004). Salt movement, tectonic events, and structural style in the central Zagros fold and thrust belt (Iran). In *Salt-Sediment Interactions and Hydrocarbon Prospectivity: Concepts, Applications, and Case Studies for the 21st Century*, 24th Annual Research Conference, GCSSEPM Foundation, 753–778.

Ndiaye, M. (2012). *Étude sismostratigraphique et sédimentologique du Bassin Sénégalo-Mauritanien dans le secteur de Diourbel et Thiès* (Doctoral thesis, Université de Genève). https://doi.org/10.13097/archive-ouverte/unige:24877

Ndiaye, M., Ngom, P. M., Gorin, G., Villeneuve, M., Sartori, M., Medou, J. (2016). A new interpretation of the deep-part of Senegal-Mauritanian basin in the Diourbel-Thies area by integrating seismic, magnetic, gravimetric and borehole data: Implication for petroleum exploration. *Journal of African Earth Sciences, 121*, 330–341. https://doi.org/10.1016/j.jafrearsci.2016.05.017

Peron-Pinvidic, G., Manatschal, G. (2009). The final rifting evolution at deep magma-poor passive margins from Iberia-Newfoundland: A new point of view. *International Journal of Earth Sciences*, *98*, 1581–1597.

Pogson, M. (2003). *Chinguetti-4-3: PVT and Water Analysis Report*. Woodside Ltd., Internal Report, DRIMS#273201. Unpublished report, Ministry of Petroleum and Energy, internal archive.

Slade, J. (2005). *Petrophysical Curve and Geolog Set Definitions*. Woodside Ltd., Internal Report, DRIMS 1991012. Unpublished report, Ministry of Petroleum and Energy, internal archive.

Société Mauritanienne des Hydrocarbures (SMH). (2024). *Développement des projets gaziers en Mauritanie: GTA, BirAllah et Banda*. https://smh.mr/fr/developpement/

Sridi, A., Aliouane, L., Doghmane, M. Z., Ouadfeul, S.-A., Boudella, A. (2023). Porosity and permeability prediction in shaly Triassic reservoirs of the Hassi R'mel Field (Algeria) from well log data using fuzzy logic. *Bulletin of Geophysics and Oceanography*. https://doi.org/10.4430/bgo00408

Sturrock, V. (2003). *Chinguetti Field Petrophysics Report*. Woodside Ltd., Internal Report, DRIMS 257323.

Tari, G., Brown, D., Jabour, H., Hafid, M., Louden, K., Zizi, M. (2012). The conjugate margins of Morocco and Nova Scotia, Canada. In D. G. Roberts A. W. Bally (Eds.), *Phanerozoic Passive Margins, Cratonic Basins and Global Tectonic Maps* (pp. 285–323). Elsevier. https://doi.org/10.1016/B978-0-444-56357-6.00011-1

Tari, G., Jabour, H. (2013). Salt tectonics along the Atlantic margin of Morocco. In *Conjugate Divergent Margins* (Geological Society, London, Special Publications, Vol. 369, pp. 337–353). Geological Society, London. https://doi.org/10.1144/SP369.18

Tari, G., Molnar, J., Ashton, P. (2003). Examples of salt tectonics from West Africa: A comparative approach. *Geological Society, London, Special Publications*, *207*, 85–104. https://doi.org/10.1144/GSL.SP.2003.207.5

Vear, A. (2005). Deep-water plays of the Mauritanian continental margin. In A. G. Dore B. A. Vining (Eds.), *Petroleum Geology: North-West Africa and Other Atlantic Margins*. Geological Society, London. https://doi.org/10.1144/0061465

Verma, A. K., Cheadle, B. A., Routray, A., Mohanty, W. K., Mansinha, L. (2012). Porosity and permeability estimation using neural network approach from well log data. In *Annual Technical Conference and Exhibition*, Society of Petroleum Engineers, San Antonio, TX, USA, 1–6. https://doi.org/10.2118/159740-MS

Willis, M. E., Burns, D. R., Rao, R., Minsley, B. J., Toksöz, M. N., Vetri, L. (2006). *Spatial orientation and distribution of reservoir fractures from scattered seismic energy*. Geophysics, 71(5), O43–O51. https://doi.org/10.1190/1.2235977.

Woodside Petroleum Ltd. (2004). *2004 Concise Annual Report*. Woodside Petroleum Ltd.